Journal of Advanced Ceramics
2024, **13**(4): 496–506
https://doi.org/10.26599/JAC.2024.9220872

Research Article

Boron nitride microribbons strengthened and toughened alumina composite ceramics with excellent mechanical, dielectric, and thermal conductivity properties

Jilin Wang[1,2,3], Dongping Lu[1], Weiping Xuan[1], Yuchun Ji[1,2], Ruiqi Chen[4], Shaofei Li[1], Wenbiao Li[1], Wenzhuo Chen[1], Shilin Tang[1], Guoyuan Zheng[1,2], Fei Long[1,2]✉

[1] *Guangxi Key Laboratory of Optical and Electronic Materials and Devices, Collaborative Innovation Center for Exploration of Nonferrous Metal Deposits and Efficient Utilization of Resources, School of Materials Science and Engineering, Guilin University of Technology, Guilin 541004, China*
[2] *Key Laboratory of New Processing Technology for Nonferrous Metals and Materials of Ministry of Education, Guilin University of Technology, Guilin 541004, China*
[3] *School of Materials Science and Engineering, Peking University, Beijing 100871, China*
[4] *Department of Civil and Environmental Engineering, The Hong Kong Polytechnic University, Kowloon 999077, Hong Kong, China*

Received: January 1, 2024; Revised: March 2, 2024; Accepted: March 2, 2024

Abstract: Aluminum oxide (Al_2O_3) ceramics have been widely utilized as circuit substrates owing to their exceptional performance. In this study, boron nitride microribbon (BNMR)/Al_2O_3 composite ceramics are prepared using spark plasma sintering (SPS). This study examines the effect of varying the amount of toughened phase BNMR on the density, mechanical properties, dielectric constant, and thermal conductivity of BNMR/Al_2O_3 composite ceramics while also exploring the mechanisms behind the toughening and increased thermal conductivity of the fabricated ceramics. The results showed that for a BNMR content of 5 wt%, BNMR/Al_2O_3 composite ceramics displayed more enhanced characteristics than pure Al_2O_3 ceramics. In particular, the relative density, hardness, fracture toughness, and bending strength were 99.95%±0.025%, 34.11±1.5 GPa, 5.42±0.21 MPa·m$^{1/2}$, and 375±2.5 MPa, respectively. These values represent increases of 0.76%, 70%, 35%, and 25%, respectively, compared with the corresponding values for pure Al_2O_3 ceramics. Furthermore, during the SPS process, BNMRs are subjected to high temperatures and pressures, resulting in the bending and deformation of the Al_2O_3 matrix; this leads to the formation of special thermal pathways within it. The dielectric constant of the composite ceramics decreased by 25.6%, whereas the thermal conductivity increased by 45.6% compared with that of the pure Al_2O_3 ceramics. The results of this study provide valuable insights into ways of enhancing the performance of Al_2O_3-based ceramic substrates by incorporating novel BNMRs as a second phase. These improvements are significant for potential applications in circuit substrates and related fields that require high-performance materials with improved mechanical properties and thermal conductivities.

Keywords: boron nitride microribbons/aluminum oxide (BNMRs/Al_2O_3) composite ceramics; boron nitride microribbon (BNMR); spark plasma sintering (SPS); strengthening and toughening; thermal conductivity

1 Introduction

With the continuous development of science and technology in the 21st century, microelectronic technology has moved toward miniaturization, lightness, and greater integration. The high complexity of integrated devices has made heat accumulation increasingly critical and has resulted in higher heat dissipation requirements for substrates and packaging materials [1]. Thermally conductive ceramic substrates are primarily used to solve the problem of heat dissipation in electronic devices. Common thermally conductive ceramic substrates are alumina ceramics, beryllium oxide ceramics, aluminum nitride ceramics, and silicon nitride ceramics [2,3]. Among these, beryllium oxide is known to produce toxic substances. In addition, aluminum nitride and silicon nitride have problems such as high sintering temperatures and difficulty in sintering and densification [4]. As the most common conductive ceramic substrate, aluminum oxide (Al_2O_3) has the advantages of high-temperature resistance, corrosion resistance, good chemical stability, wear resistance, and low density; further, there is a wide range of raw material sources at low prices. However, there are also certain problems in the development and use of alumina ceramic thermally conductive substrates [5–7]. Firstly, There remains considerable scope for improvement in the mechanical properties of alumina ceramics, particularly in terms of their hardness, fracture toughness, and strength. Secondly, the thermal conductivity of alumina ceramics cannot meet the heat dissipation requirements of modern new-generation electronic devices. Thirdly, their ion bonds are strong, resulting in a low particle-diffusion coefficient and relatively harsh sintering conditions. These problems have thus limited the development of alumina ceramics for application in precision mechanical functional ceramics.

Considering the problems associated with the mechanical

✉ Corresponding author.
E-mail: longf@glut.edu.cn

properties of alumina ceramics, composite materials have been used to design and prepare multiphase ceramics to solve the strengthening and toughening problems of alumina ceramics [8]. Toughening methods for alumina ceramics mainly include particle and whisker toughening. Particle toughening involves the addition of second-phase particle materials to alumina-based ceramics to improve their toughness. The main mechanisms of whisker toughening in alumina ceramics are crack deflection, fiber bridging, and the pull-out effect. Chen *et al.* [9] added 0.2 wt% graphene nanosheets (GNSs) using hot-pressing technology and the mechanism of whisker toughening. The composite ceramics had the highest K_{IC} at 1500 ℃, reaching 6.6 MPa·m$^{1/2}$, which was approximately 43.5% higher than that of the blank sample. Wang *et al.* [10,11] used boron nitride nanotubes (BNNTs) as the reinforcing phase and α-Al_2O_3 as the starting materials to prepare BNNTs/Al_2O_3 composites by hot pressing sintering. The addition of sodium dodecyl sulfate (SDS) as a dispersant improved the dispersion of BNNTs. They found that a small amount of chemical reaction between BNNTs and Al_2O_3 could also improve the interfacial bonding. The relative densities of samples containing 1.5 wt% BNNTs reached 98.0%. However, the high-pressure technique and long sintering cycle (6 h) promoted the continuous growth of grains, which is not conducive to obtaining dense alumina ceramics.

With respect to the thermal conductivity problem of alumina ceramics, the principle of improving the thermal conductivity of ceramics involved increasing the mean free path of phonons. The greater the number of defects, impurities, and grain boundaries in the crystal, the stronger the scattering of elastic waves. This results in a smaller free path of phonons and, consequently, a lower thermal conductivity of the ceramics [12–15]. Three methods can be used to improve the thermal conductivity of Al_2O_3 ceramics: (1) the removal of excess impurities from ceramics; (2) increasing the relative density of the ceramics to reduce the number of pores in the matrix, which in turn will affect the scattering of phonons; (3) addition of a second phase in Al_2O_3-based ceramics, which could show better thermal conductivity when the two phases are isolated from each other. Hexagonal boron nitride (h-BN) displays excellent thermal conductivity (the theoretical thermal conductivity is approximately 300 W/(m·K)). Hence, it is usually added to ceramics as a common thermally conductive second phase to improve the thermal conductivity of multiphase ceramics. For example, Liu *et al.* [16] added 20 wt% h-BN as the additive phase and 5 wt% Y_2O_3 as the sintering aid. Through hot press sintering, when the sintering temperature reached 1900 ℃, the thermal conductivity of the AlN/BN composite ceramics was 98.3 W/(m·K). Kim *et al.* [5] added a small amount of 0.3 wt% BNNTs to yttria-stabilized zirconia-toughened alumina (YZTA) ceramics. The thermal conductivity of the resulting composite ceramics ranged from 20.7 to 21.4 W/(m·K). The thermal conductivity of YZTA–BNNT composite ceramics depended on the amount of BNNT added. Therefore, h-BN has good potential for application to increase the thermal conductivity of ceramics [17–24].

Hence, h-BN/Al_2O_3 composite ceramics show good potential for application in thermally conductive ceramic substrates. However, h-BN/Al_2O_3 composite ceramics also have some limitations. First, most of the toughening phases are BNNTs, which are nanotubes with relatively large lengths and diameters. They do not easily or uniformly disperse in the alumina powders, and dispersants are often used. Second, the raw materials mostly used are submicron or nanometer alumina powders, which are expensive.

To address the challenges related to BN/Al_2O_3 thermally conductive composite ceramic substrates, our group aimed to use novel boron nitride microribbons (BNMRs) as the second phase. The morphology of a material influences its intrinsic physical and chemical properties. For example, one-dimensional (1D) boron nitride micron materials as an additive phase contribute more to the toughness of the composite, which has the characteristics of high tensile strength and elastic modulus, large Young's modulus, good insulation, low dielectric constant, high-temperature resistance, good thermal conductivity, and good chemical properties [25–30]. Unidimensional boron nitride (BN) materials have a faster phonon transport capability per unit space, which can significantly improve the thermal conductivity of composites. The characteristics of boron nitride 1D micron materials can be harnessed, and appropriate sintering methods can be adopted to enhance their mechanical properties while enhancing the thermal conductivity of the composite materials. Therefore, the preparation of high-thermal-conductivity BN/Al_2O_3 composite ceramics with excellent mechanical properties is feasible. This study provides new ideas for the development of Al_2O_3-based thermally conductive composite ceramic substrates with important research significance.

In this study, novel homemade BNMRs were used as the toughened phase to prepare BNMR/Al_2O_3 high-performance composite ceramics by spark plasma sintering (SPS). BNMRs exhibit micron-scale diameters, suitable aspect ratios, and have an excellent toughening effect. The effects of the BNMR content on the phase, microstructure, and mechanical, thermal, and electrical properties values of BNMR/Al_2O_3 composite ceramics were investigated. The toughening mechanism and thermal conductivity of BNMR/Al_2O_3 composite ceramics were also discussed.

2 Experimental

2.1 Preparation of BNMRs

BNMRs are homemade 1D h-BN strip solid materials with a width of 1–2 μm (Fig. 1). The precursors were prepared from zinc borate ($B_{12}H_{18}O_{29}Zn_4$) via a hydrothermal reaction [31]. An appropriate amount of precursor was obtained and placed in a tube furnace. The tube furnace was evacuated and charged with NH_3. Next, the temperature was increased to 1150 ℃ and maintained for 5 h to obtain BNMRs [32].

2.2 Pretreatment of mixed raw materials

Commercial grade Al_2O_3 powders (99.99%) with a particle size of 3–4 μm were used. Al_2O_3 was put into a muffle furnace (KSL-1700X, Hefei Kejing Material Technology Co., Ltd., China), heated to 1200 ℃ for 2 h, and then cooled naturally to obtain Al_2O_3 powders. The purpose of the pretreatment of Al_2O_3 powders was to stabilize the phase, remove other impurities from the surface, and limit their effect on the subsequent sintering process. Then, Al_2O_3 was mixed with homemade BNMRs at a certain ratio, and the powders were placed in a planetary ball mill (TG16-WS, Hunan Saite Xiangyi Centrifuge Instrument Co., Ltd., China) with a ball-to-material ratio of 1 : 5 using absolute ethanol as a dispersant. This was done at a speed of 200 r/min and for a mixing time of 20 h. The powder samples were dried in a vacuum drying oven (DZF-6020, Shanghai Qixin Science Equipment Co., Ltd., China) at 80 ℃.

2.3 Preparation of composite ceramic SPS sintering

The raw materials were placed in a high-strength graphite mold

with an inner diameter of 20 mm and sintered in a spark plasma sintering furnace (SPS-10t-5, Shanghai Chenhua Technology Co., Ltd., China) under vacuum at less than 10 Pa. The firing process was as follows: The temperature was increased to 1400 ℃ at a rate of 50 ℃/min and then increased to 1450–1550 ℃ at a rate of 10 ℃/min. During SPS, the pressure was gradually increased; the final holding pressure was 75 MPa, and the holding time was 18 min. Finally, BNMR/Al_2O_3 composite ceramics of diameter 20 mm and thickness 2 mm were prepared (Fig. 2 and Fig. S1 in the Electronic Supplementary Material (ESM)).

2.4 Performance test

Next, the ceramic samples were polished using an automatic pressure polishing machine. The relative densities of the samples were measured using the drainage method according to Archimedes' principle. After coarse polishing, fine polishing, ultrasonic cleaning, and drying of the ceramic samples, the hardness of the samples was measured with a Vickers hardness tester (EV-1000L). The pressure load was 1500 g, and the pressure was applied and held for 20 s. At this time, the diagonal length value of indentation and crack was measured by the metallography microscope software to calculate the fracture toughness value. The fracture toughness value of the test sample was calculated by the equation: $K_{IC} = 0.06673 H_V^{0.6} E^{0.4} a^2 c^{-1.5}$, where K_{IC} is the fracture toughness of the test sample (MPa·m$^{1/2}$), H_V is the Vickers hardness of the test sample, and E is the elastic modulus of the sample. $2a$ is the diagonal length of the square indentation, $2c$ is the diagonal length of the crack, and the crack length should satisfy the condition $a/c \leq 0.4$. The three-point bending strengths of the samples were measured using a universal material-testing machine (DDL200KN, Changchun Research Institute for Mechanical Science Co., Ltd., China). The dielectric constant of the BNMRs/Al_2O_3 composite ceramics was measured as a function of temperature using an impedance analyzer (Agilent 4294A, Agilent Inc., USA). The thermal conductivity of the BNMR/Al_2O_3 composite ceramics was measured using a hot disk (Hot Disk TPS 2500S, Hot Disk AB Company, Sweden). The phase of the BNMR/Al_2O_3 composite ceramics was analyzed by an X-ray diffractometer (XRD; X'Pert PRO, PANalytical B.V., the Netherlands). The microstructure of the composite ceramic samples was observed using a transmission electron microscope (TEM; JEOL-2010F, Japan). The surface and section were characterized using a scanning electron microscope (GeminiSEM 300, Carl Zeiss, Germany; S-4800, Hitachi, Japan). The energy

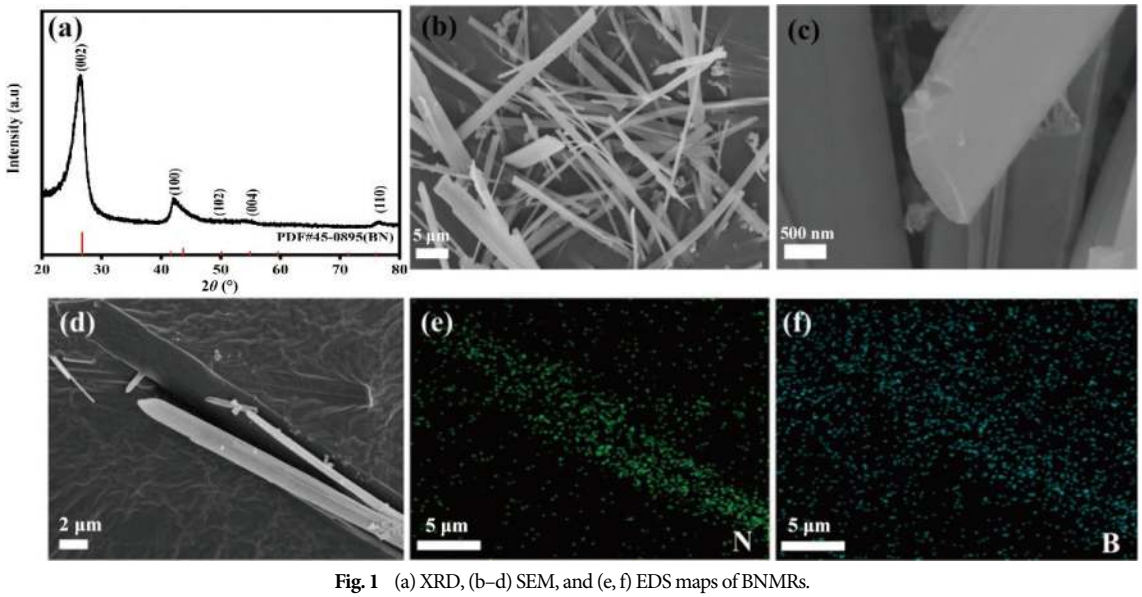

Fig. 1 (a) XRD, (b–d) SEM, and (e, f) EDS maps of BNMRs.

Fig. 2 BNMRs/Al_2O_3 composite ceramic preparation process.

dispersive X-ray spectrometry (EDS) profile of the sample was characterized by an EDS spectroscope (INCA IE 350 PentaFET X-3, Oxford, UK), which is included with Zeiss electron microscopy.

3 Results and discussion

3.1 Effect of BNMRs content on the phase of BNMRs/Al_2O_3 composite ceramics

Figure 3 shows the XRD patterns of the best Al_2O_3 composite ceramic samples with different BNMR contents fired at different temperatures and relative densities of 99% or more. Each composite ceramic sample consisted of only Al_2O_3 (PDF#46-1212) and BN (PDF#45-0895), with no other impurity phases. There was no chemical reaction between BN and Al_2O_3. The intensity of the main diffraction peak of the h-BN phase increased with increasing h-BN content. The sharp diffraction peak, high diffraction intensity, and small full width at half maximum (FWHM) show that the Al_2O_3 grains had good crystallinity.

3.2 Effect of BNMRs content on microstructure of BNMRs/Al_2O_3 composite ceramics

Figure 4 shows the surface morphology of the BNMR/Al_2O_3 composite ceramics after thermal etching in a muffle furnace (KSL-1700X, Hefei Kejing Material Technology Co., Ltd., China) at 1400 ℃ for 30 min under an air atmosphere. Figure 4(a) presents the surface morphology of the pure phase Al_2O_3 ceramics. The grains were large, and abnormal grain growth was accompanied by a few small grains. After the addition of BNMRs,

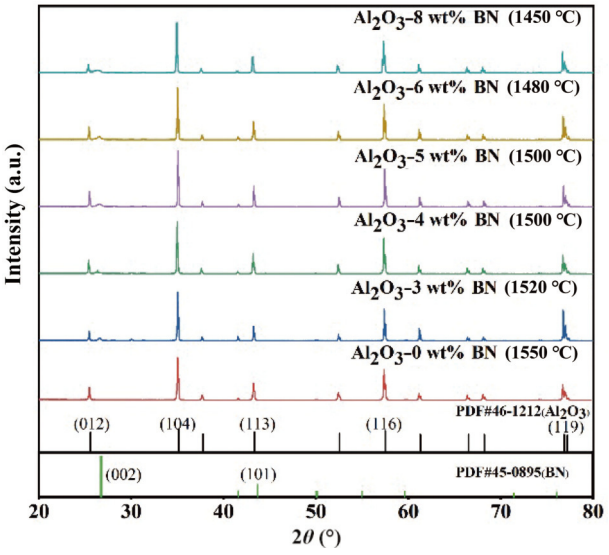

Fig. 3 XRD patterns of BNMRs/Al_2O_3 composite ceramics with different BNMRs contents.

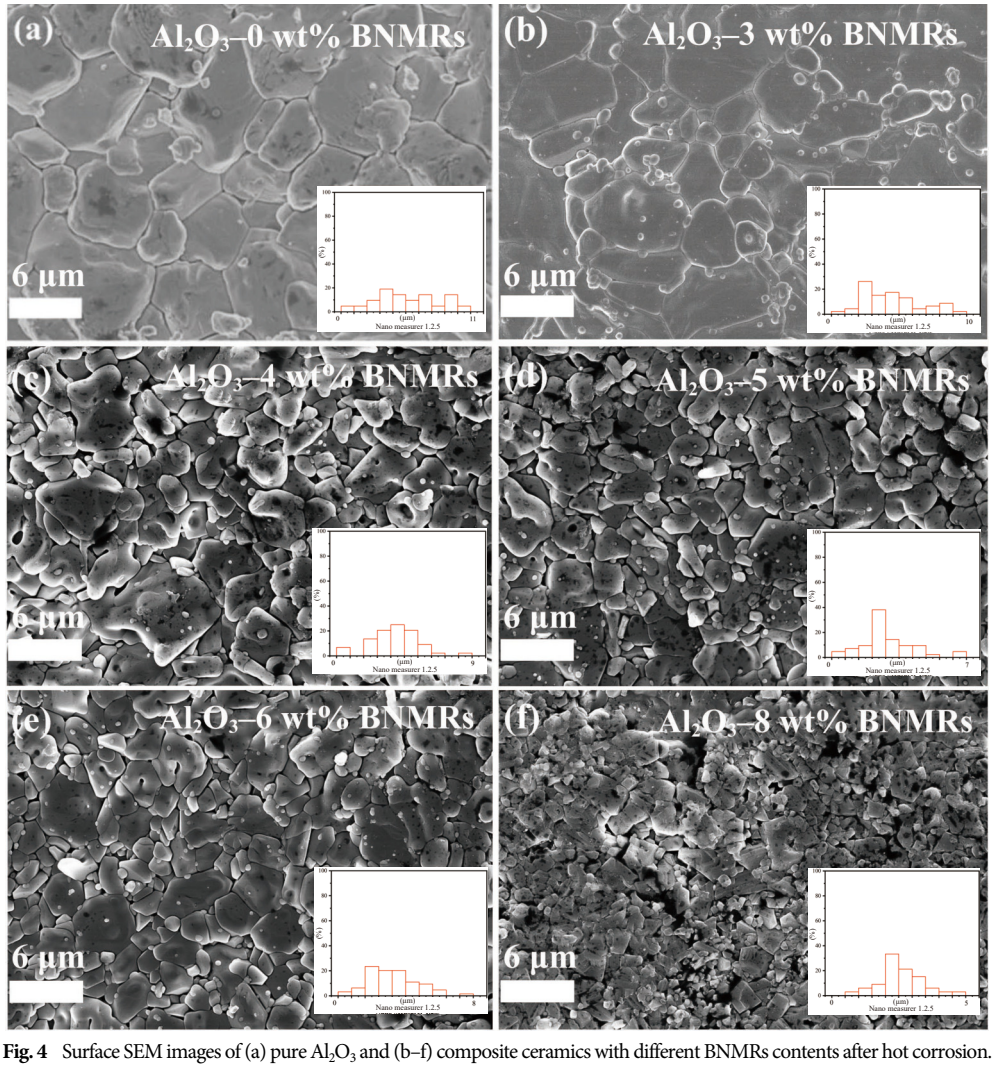

Fig. 4 Surface SEM images of (a) pure Al_2O_3 and (b–f) composite ceramics with different BNMRs contents after hot corrosion.

the grains showed significant refinement, and the size decreased significantly with the increase of mass fraction (from 3–6 to 1–2 μm) (Figs. 4(b)–4(f)).

The BNMR/Al_2O_3 composite ceramic powders with a BNMR content of 5 wt% are shown in Fig. 5(a). The grain size of Al_2O_3 was 2–3 μm, and the width of BNMRs was 1–2 μm. The BNMRs were evenly dispersed in the Al_2O_3 powders. A sectional pore analysis of BN/Al_2O_3 composite ceramics with different BNMR contents is shown in Fig. 5. Compared with pure Al_2O_3 ceramics, the BN/Al_2O_3 composite ceramics had fewer closed pores, and the relative density was improved, which indicates that a moderate amount of toughened phase BNMRs could facilitate the densification of the Al_2O_3 ceramics. In addition, the Al_2O_3 grain size of composite ceramics was 1–2 μm, which is smaller than that of pure Al_2O_3 ceramics (3–4 μm). This indicates that the toughened phase BNMRs could inhibit the excessive growth of Al_2O_3 grains effectively.

The flat section of the pure Al_2O_3 ceramics exhibited a typical mixed intergranular and transgranular fracture mode (Fig. 5(b)). The Al_2O_3 grains with larger grain sizes showed a smooth transgranular fracture mode, whereas the Al_2O_3 grains with smaller grain sizes displayed an angular intergranular fracture mode. During the sintering process, a large number of oxygen vacancies were generated, resulting in the reduction of the grain boundary strength and the formation of intergranular fractures [33,34]. As the BNMR content increased, the section surface became uneven (Figs. 5(c)–5(j)), which is a typical intergranular fracture mode. When the BNMR content was 5 wt%, an obvious bridging effect of the BNMRs was observed (Fig. 5(f)). BNMRs are micron-long ribbons with good dispersion and excellent flexibility, enabling BNMRs to wrap easily around the surfaces of Al_2O_3 grains at high temperatures and pressures (Figs. 5(g) and 5(h)). When the BNMR content increased (Figs. 5(i) and 5(j)), a small number of pores appeared. The fracture mode was intergranular, which was also proven by the decrease in mechanical properties. In the SPS process, an increase in the BNMR content caused agglomeration, resulting in an uneven distribution of BNMR and Al_2O_3 particles, affecting the plastic flow and mass transfer process in the later stage. This is not conducive to sintering densification and reduces the density of the composite ceramics. As the BNMR content increased (as shown by the yellow box in Fig. 5(j)), the BNMRs agglomerated, resulting in a pore size at the junction between the nanoribbons and matrix [35].

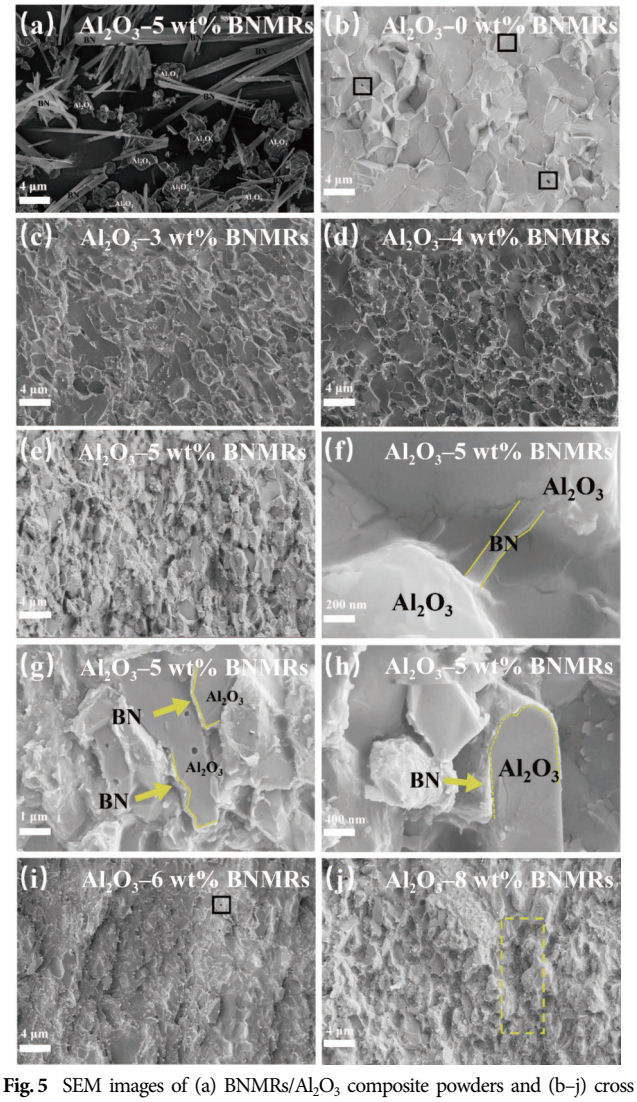

Fig. 5 SEM images of (a) BNMRs/Al_2O_3 composite powders and (b–j) cross sections of BNMRs/Al_2O_3 composite ceramics with different BNMRs contents.

Figures 6(a) and 6(b) show the cross-sectional EDS maps of the Al_2O_3–5 wt% BNMR composite ceramics prepared at a sintering temperature of 1500 ℃ for a holding time of 18 min. The distribution of BN in the composite ceramics was determined based on the distributions of B and N. The contents of Al and O at the grain boundary decreased, but the contents of B and N increased. The BNMRs were distributed at the grain boundaries between the Al_2O_3 grains, which wrapped around the Al_2O_3 grains and played a pinning role. It not only inhibited the growth of Al_2O_3 grains and slowed the movement rate of Al_2O_3 grain boundaries but also strengthened the grain boundaries, thus improving the fracture toughness of the composite ceramics.

Figures 7(a) and 7(b) show TEM and high-resolution transmission electron microscope (HRTEM) images of the BNMR/Al_2O_3 composite ceramics. Many banded structures were coated around the grains (Fig. 7(a)). In Fig. 7(b), the lattice fringes of the BNMRs are clearly distinguishable, and the crystal plane spacing is 0.334 nm, which is consistent with the (002) crystal plane spacing of h-BN. In addition, the crystal plane spacing of 0.35 nm is consistent with the (012) crystal plane of α-Al_2O_3. According to the corresponding EDS maps of Al, O, N, and B (Figs. 7(c)–7(f)), the surface of the Al_2O_3 grain was wrapped by uniform BNMRs with high purity and crystallinity. Despite the bending shapes of the Al_2O_3 grains, the BNMRs could still closely coat their surface and extend outward to wrap other Al_2O_3 grains. Therefore, BNMRs can inhibit the growth of Al_2O_3 grains. The special thermal conductivity pathways of BN in the composite ceramics may significantly increase the thermal conductivity of BNMRs/Al_2O_3 composite ceramics.

3.3 Effect of BNMRs on relative density and mechanical properties of BNMRs/Al_2O_3 composite ceramics

With an increase in the BNMR content, the sintering temperature of the BNMR/Al_2O_3 composite ceramics decreased (Fig. 8(a)). When the optimum sintering temperature was exceeded, the composite ceramics overfired, resulting in a decreased sample density. When the sintering temperature was 1500 ℃ and the BNMR content was 5 wt%, the relative density of the composite ceramics could reach 99.95%±0.025%, which is 0.76% higher than that of pure Al_2O_3 ceramics. The BNMR width may have been smaller than that of the Al_2O_3 grains. During sintering, the BNMRs easily filled the pores between the Al_2O_3 grains. The appropriate number of BNMRs uniformly linked together in

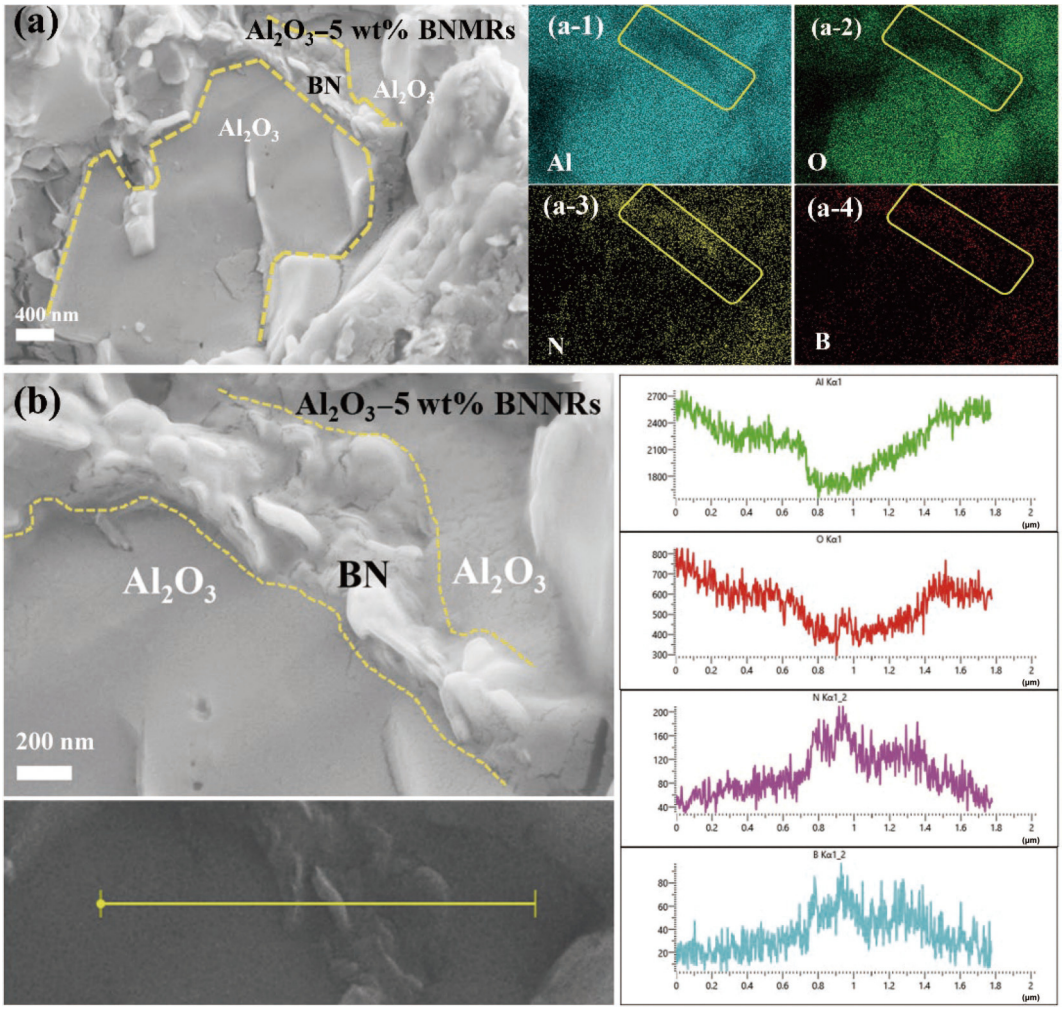

Fig. 6 EDS maps of fracture surface in BNMRs/Al_2O_3 composite ceramics: (a) EDS surface scanning maps and (b) line scanning maps.

different arrangement modes partially inhibited the diffusion of Al_2O_3 particles, which was beneficial for the reduction of pores during the sintering process. When the content of BNMRs continued to increase, although the sintering temperature decreased, the relative density was 99.39%±0.026%, which is because of the agglomeration of BNMRs, resulting in the increased pores and decreased relative density.

The hardness of the composite ceramics first increased and then decreased (Fig. 8(b)). When the BNMR content reached 5 wt%, the hardness reached the maximum value (34.11±1.5 GPa), which is 70% higher than that of pure Al_2O_3 ceramics. With a further increase in the BNMR content, the BNMR agglomerated, reducing the density and hardness of the composite ceramics.

Similarly, when the BNMRs content was 5 wt%, the maximum fracture toughness was observed and reached 5.42±0.21 MPa·$m^{1/2}$, which is 35% higher than that of pure Al_2O_3 ceramics (Fig. 8(c)). This is because the BNMRs treated with an appropriate amount of anhydrous ethanol were evenly distributed at the Al_2O_3 grain boundaries. As the crack expanded, the intergranular fracture mode caused the crack to turn, producing branching cracks, microcracks, and lattice changes. These cracks continuously consumed the energy of the crack expansion and improved the fracture toughness. Moreover, because 1D h-BN has excellent mechanical properties, such as high elastic modulus and flexural strength, it can deflect cracks and hinder crack propagation [36]. In addition, the bridging effect of the BNMRs at the fracture site improved the fracture properties of the composite ceramics. However, when the BNMR content was increased to 8 wt%, the BNMRs appeared agglomerated, and the number of pores increased, inducing crack propagation and reducing fracture toughness.

As shown in Fig. 8(c), when the addition amount was 5 wt%, the bending strength also reached the maximum value (375±2.5 MPa), which is 25% higher than that of pure Al_2O_3 ceramics. An appropriate BNMR content could inhibit the growth of Al_2O_3 and refine the grains. Figure 5(g) shows that BNMRs play the role of bridging, nailing, and wrapping Al_2O_3 grains, strengthening the grain boundaries between Al_2O_3 and BNMRs, which significantly improved the bending strength of the composite ceramics.

3.4 Effect of BNMRs on dielectric constant of BNMRs/Al_2O_3 composite ceramics

The variation of dielectric constant (1 MHz) and dielectric loss (1 MHz) of BN/Al_2O_3 composite ceramics with different BNMR contents at room temperature (30–100 ℃) is shown in Fig. 9. The dielectric constant initially decreased and then increased as the BNMR content increased (Fig. 9(a)). The variation of dielectric constant may have been influenced by the following factors: i) Owing to the pores present in ceramics, composite ceramics with low relative density would display a low relative dielectric constant; ii) when the BNMR content is less than 5 wt%, the large grain size renders it difficult to remove oxygen vacancies from the

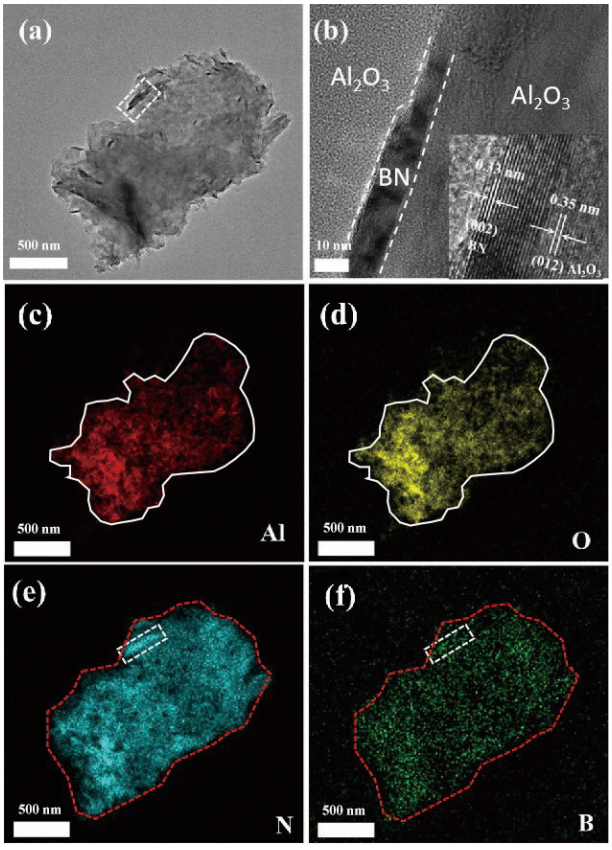

Fig. 7 (a) TEM, (b) HRTEM, and (c–f) corresponding EDS maps of BNMRs/Al_2O_3 composite ceramics.

grains, causing defects and lower dielectric constant [37,38]; iii) the smaller grain size tends to produce more grain boundaries, resulting in a greater space charge, increasing the dielectric loss and the dielectric constant; iv) BN has a significantly lower dielectric constant (ε_γ = 3–4.4) than Al_2O_3, resulting in a decrease in the dielectric constant of BNMRs/Al_2O_3 composite ceramics [16,9,39–44]. However, with an increase in the filler content, BN was dispersed in the Al_2O_3 matrix more evenly, and the relative density of the composite ceramics increased. The interface between the filler and the Al_2O_3 matrix increased, the interface polarization increased, and the dielectric constant of the composite ceramics increased. When the BNMR content was 5 wt%, the dielectric constant of the composite ceramics was 6.18±0.02. However, with an increase in the BNMR content, BNMRs exhibited random interleaving and agglomeration, defects increased, and the relative density and polarization ability decreased, finally leading to a decreased dielectric constant. The dielectric loss of the sample increased with the increase of BN content (Fig. 9(b)), which is because the relative density of the sample decreased, and the density of BN powders was lower than that of Al_2O_3 powders. As the BN content increased, additional impurity elements were introduced into the BNMRs/Al_2O_3 system, thus increasing the point defects in the sample and the dielectric loss of the BNMRs/Al_2O_3 composite.

3.5 Effect of BNMRs on thermal conductivity of BNMRs/Al_2O_3 composite ceramics

According to Fig. 10, the thermal conductivity of composite ceramics at 25 ℃ first increased and then decreased. The changing trend was the same as that of the mechanical and dielectric constants. When BNMRs were introduced to the Al_2O_3 matrix, the wrapped alumina grains were gradually refined, increasing the number and area of grain boundaries. This increased the strength of the lattice vibrations, reduced the mean free path of the phonons, and improved the thermal conductivity.

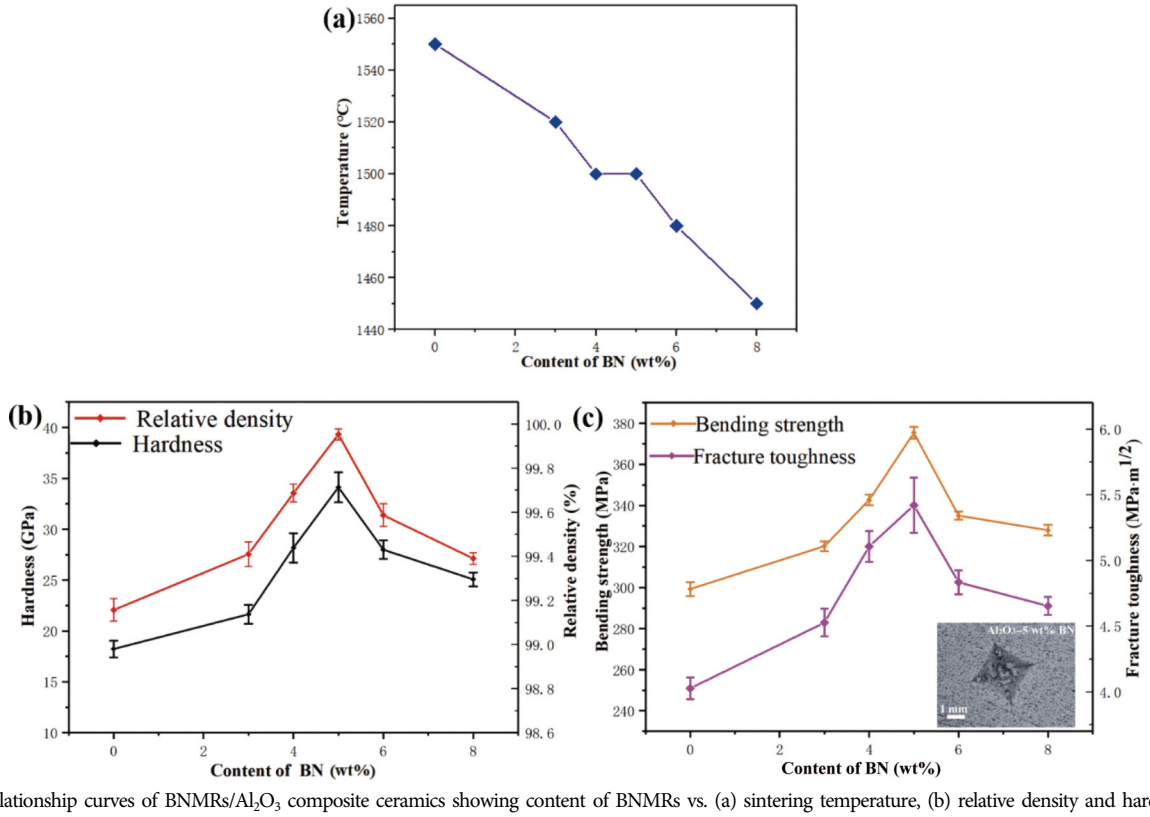

Fig. 8 Relationship curves of BNMRs/Al_2O_3 composite ceramics showing content of BNMRs vs. (a) sintering temperature, (b) relative density and hardness, and (c) fracture toughness and bending strength.

The more uniform the BN coating on Al_2O_3, the fewer the number of defects, such as dislocations and pores, in the ceramics. This could be beneficial for the formation of special BNMR pathways to improve phonon transport, effectively reduce phonon scattering, and increase thermal conductivity [45]. Notably, fewer BNMRs dispersed in the matrix will be unable to fabricate a complete thermal conduction path, resulting in a low rate of increase in the thermal conductivity coefficient.

As the BN content continuously increased, the relative density also continued to increase. The closer the contact between BN and the Al_2O_3 matrix, the more the thermal conductivity increased, reaching a maximum value of 15.89±0.13 W/(m·K). Compared with that of pure Al_2O_3 (10.91±0.10 W/(m·K)), the thermal conductivity increased by 45.6%. When the BNMR content exceeded 5 wt%, the BNMRs agglomeration introduced new defects, the relative density decreased, and the porosity increased. Pores were encountered in the process of lattice vibration, resulting in an "annihilation" effect, which weakened the lattice vibration and reduced the mean free path of phonons, thus causing the thermal conductivity to decrease.

To further evaluate the thermal conductivity of BNMRs/Al_2O_3 composite ceramics, infrared imaging tests were performed on a heating table preheated at 80 ℃. Figure 10(b) shows the variation of temperature with time at the composite ceramic center with a surface area of 3.14 cm^2. With increasing BNMR content, the thermal response speed of the BNMRs/Al_2O_3 composite ceramics first increased and then decreased. In particular, when the BNMR content was 5 wt%, the center point of composite ceramics could reach a maximum of 77.1 ℃ within 30 s, and the heat distribution was the most uniform.

3.6 Toughening and thermal conduction mechanism of BNMRs/Al_2O_3 composite ceramics

A schematic of the proposed toughening and heat conduction mechanism of the BNMRs/Al_2O_3 composite ceramics is shown in Fig. 11. The Al_2O_3 and BNMRs were uniformly dispersed after the ball milling process (Figs. 11(a) and 11(b)). During the sintering process, the pliable BNMRs were continuously extruded and deformed by the Al_2O_3 grains under high temperature and pressure (Fig. 11(c)), followed by even wrapping of the Al_2O_3 grains (Fig. 11(d)). The BNMRs distributed between the Al_2O_3 grain boundaries reduced the atomic diffusion coefficient and inhibited the potential abnormal growth of Al_2O_3 grains.

By referring to the literature, it can be deduced that the main toughening methods of alumina composite ceramics are crack propagation resistance, dispersion strengthening, crack deflection, fiber bridging, fiber pulling out, etc. [46–48]. The crack photographs indicated crack deflection, micro-crack, fiber pulling out, and bridging (Figs. 12(a)–12(c) and Fig. S3 in the ESM), which were confirmed by previous relevant literature. Simultaneously, BNMRs also play the role of bridging and pinning, resulting in strong interfacial bonding between BNMRs and the

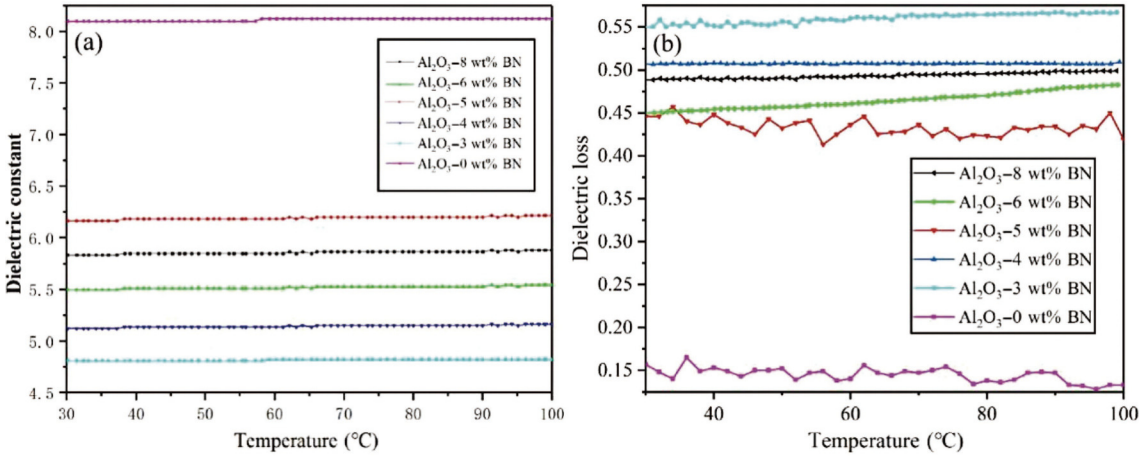

Fig. 9 Relationship curves of BNMRs contents with (a) dielectric constant and (b) dielectric loss in BNMRs/Al_2O_3 composite ceramics.

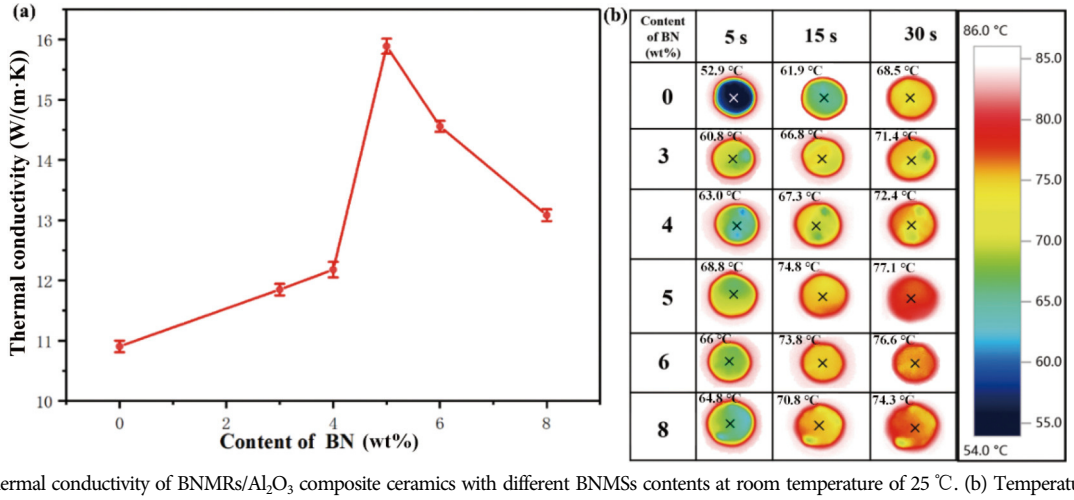

Fig. 10 (a) Thermal conductivity of BNMRs/Al_2O_3 composite ceramics with different BNMSs contents at room temperature of 25 ℃. (b) Temperature variation of composite ceramics with time.

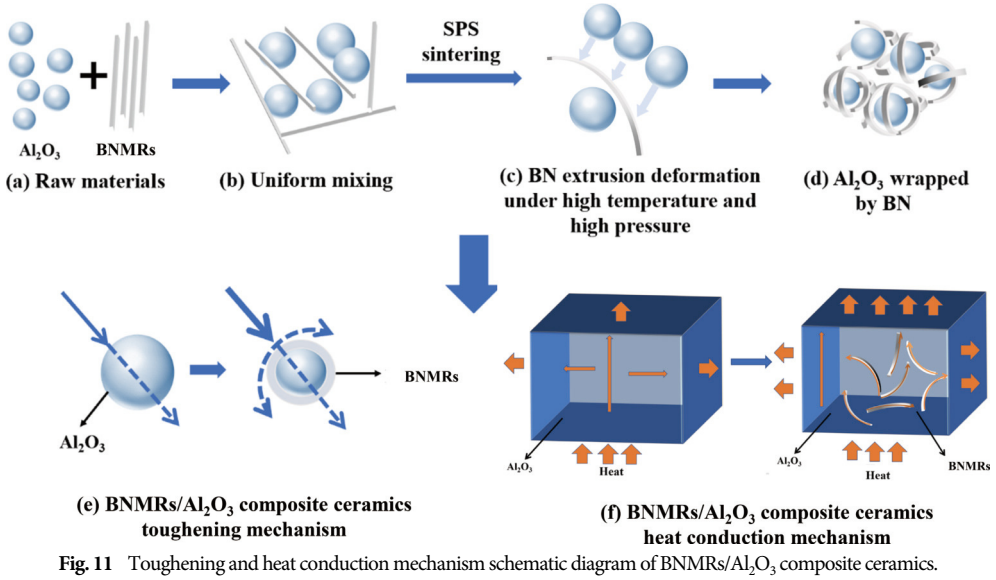

Fig. 11 Toughening and heat conduction mechanism schematic diagram of BNMRs/Al_2O_3 composite ceramics.

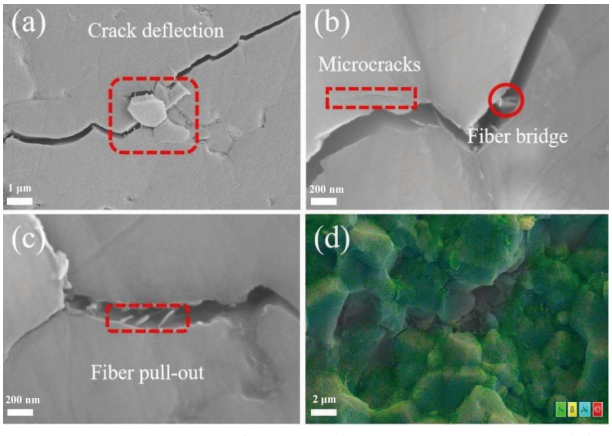

Fig. 12 (a–c) SEM images of BNMRs/Al_2O_3 composite ceramic polishing surface and (d) fracture surface EDS image of BNMRs/Al_2O_3 composite ceramic.

Al_2O_3 matrix. In addition, the uniformly distributed 1D BNMRs between the Al_2O_3 grains could improve the compactness and hinder crack propagation, increase the crack propagation distance by dispersing stress, resist higher stress, and improve the mechanical properties of BNMRs/Al_2O_3 composite ceramics (Fig. 11(e)).

However, in terms of the thermal conduction property, uniformly distributed and wrapped 1D BNMRs could fabricate special multidimensional BN high thermal conductivity networks on the surface of Al_2O_3 grains, significantly increasing the thermal conduction effect of the BNMRs/Al_2O_3 composite ceramics (Fig. 11(f)). Before, we also tried to describe these thermal conductivity pathways by backscattering SEM, but it was difficult to distinguish BN and Al_2O_3 in backscattering SEM images. Then, EDS mapping results also clearly displayed the thermal conductivity pathways constructed by BN (Fig. 12(d) and Figs. S2 and S4 in the ESM), ultimately resulting in a significant increase in the thermal conduction effect of BNMRs/Al_2O_3 composite ceramics. When the BNMR content exceeded 5 wt%, the excess BNMRs agglomerated and introduced a number of defects into the matrix. This agglomeration led to increased porosity and reduced the relative density, mechanical properties, and thermal conductivity of the BNMR/Al_2O_3 composite ceramics.

3.7 Comparison with previous results

Table 1 shows the best sample preparation process and relevant mechanical parameters obtained from the literature for typical toughened Al_2O_3 ceramics [11,49–52]. The particle size of Al_2O_3 powders used in the reported literature was less than 1 μm, whereas the Al_2O_3 used in our work was commercial powders with a particle size in the range of 3–4 μm. Compared with the Al_2O_3 powders used in the literature, the raw materials were inexpensive and easy to obtain, had low particle size requirements, and offered a wide range of applications. In addition, Al_2O_3 composite ceramics with high relative densities and good comprehensive properties can be sintered without the use of special mixing methods and sintering additives.

During SPS, the BNMRs uniformly dispersed and wrapped the Al_2O_3 grains, which inhibited the growth of Al_2O_3 grains. In

Table 1 Relevant literature on toughened Al_2O_3 ceramics

Ref.	Wang *et al.* [11]	Zhu *et al.* [51]	Klimczyk *et al.* [49]	Jaafar *et al.* [50]	Yin *et al.* [52]	This work
Average particle size of Al_2O_3	> 1 μm	0.5 μm	100 nm	1 μm	1–3 μm	3–4 μm
Sintering method	HP	HP	SPS	SPS	HP	SPS
Toughening phase and its content	1.5 wt% BNNTs+SDS	1.5 wt% graphene	15 wt% ZrO_2+20 wt% cBN	5 wt%SiC	6.9 wt% BNMSs	5 wt% BNMSs
Sintering atmosphere	Ar	—	Ar	—	N_2	—
Heating rate (℃/min)	20	—	100	400	—	50
Holding time (min)	60	60	4	4	—	18
Sintering temperature (℃)	1500	1550	1300	1500	1550	1500
Sintering pressure (MPa)	—	40	63	80	30	75
Vickers hardness (GPa)	—	21.3	20.7±1.2	21.16	21.3	34.11±1.5
Fracture toughness (MPa·m$^{1/2}$)	6.1	7.5	5.4±0.5	—	5.18	5.42±0.21

addition, 1D BNMRs exhibited excellent mechanical properties and could produce fiber pulling out, crack deflection, bridging, and pinning synergistic toughening effects when added to Al_2O_3 ceramics. Moreover, BNMRs had high thermal conductivity, which formed special phonon transport networks in the Al_2O_3 ceramics and increased their thermal conductivity. Therefore, the BNMR/Al_2O_3 composite ceramics with high density, hardness, fracture toughness, and low dielectric constant prepared in this study have the advantages of a simple preparation process, low cost, large particle size of raw materials, and no sintering additives. They are suitable for ceramic substrates with high thermal conductivities and excellent performance.

4 Conclusions

BNMRs/Al_2O_3 composite ceramics were prepared by SPS using commercial Al_2O_3 and homemade BNMRs as the toughening phase. The appropriate addition of toughened phase BNMRs can improve the properties of Al_2O_3-based ceramics and can be better used as high-thermal-conductivity substrate materials. When the added BNMR content was 5 wt%, the comprehensive performance of the BNMR/Al_2O_3 composite ceramics was a maximum. BNMRs improved the binding energy of the Al_2O_3 interface and enhanced the polarization effect. The mechanical properties of Al_2O_3-based ceramics were also improved by the fiber pulling out, crack deflection, bridging, and pinning synergistic toughening effects of BNMRs. 1D BNMRs were uniformly wrapped on the surface of Al_2O_3 grains, which had a pinning and bridging effect, inhibiting the growth of alumina grains, and forming special thermal conductivity networks. Therefore, the relative density, hardness, fracture toughness, and bending strength were respectively 99.95%±0.025%, 34.11±1.5 GPa, 5.42±0.21 MPa·$m^{1/2}$, and 375±2.5 MPa, which are increases of 0.76%, 70%, 35%, and 25% over those of pure Al_2O_3 ceramics, respectively. The dielectric constant and thermal conductivity were 6.18±0.02 and 15.89±0.13 W/(m·K), respectively. Compared with that of the pure Al_2O_3 ceramics, the dielectric constant decreased by 25.6%, and the thermal conductivity increased by 45.6%. The results of this study are expected to provide novel experimental and theoretical references for improving the overall performance of alumina-based ceramic substrates with high thermal conductivity.

Acknowledgements

The authors acknowledge the financial support from National Natural Science Foundation of China (No. 52262010), the Guangxi Natural Science Foundation of China (No. 2023GXNSFAA026384), and the Guilin Scientific Research and Technology Development Program (No. 2020011203-3).

Declaration of competing interest

The authors have no competing interests to declare that are relevant to the content of this article.

Electronic Supplementary Material

Supplementary material is available in the online version of this article at https://doi.org/10.26599/JAC.2024.9220872.

References

[1] Tong H, Zang LK, Xu J. Application of thermally conductive insulating materials in power electronics packaging. *Insul Mater* 2021, **54**: 1–9. (in Chinese)

[2] Ma ZX, Han YL, Wang N, *et al.* Microstructure of Al_2O_3+cordierite+AlN composite ceramics. *Adv Mater Res* 2013, **833**: 165–168.

[3] Wang XF, Wang RC, Peng CQ, *et al.* Synthesis and sintering of beryllium oxide nanoparticles. *Prog Nat Sci Mater Int* 2010, **20**: 81–86.

[4] Chiu HT, Sukachonmakul T, Wang CH, *et al.* Fabrication and characterization of silicon-based ceramic/aluminum nitride as thermally conductive hybrid filler in silicone rubber composite. *Mater Chem Phys* 2014, **147**: 11–16.

[5] Kim CH, Go EB, Kim HT. Thermophysical properties of zirconia toughened alumina ceramics with boron nitride nanotubes addition. *Heat Transf Eng* 2020, **41**: 1354–1364.

[6] Zhong B, Zhao GL, Huang XX, *et al.* Microstructure and mechanical properties of ZTA/BN machinable ceramics fabricated by reactive hot pressing. *J Eur Ceram Soc* 2015, **35**: 641–649.

[7] Funahashi Y, Xin YZ, Kato K, *et al.* Enhanced electrical property of graphite/Al_2O_3 composite fabricated by reductive sintering of gel-casted body using cross-linked epoxy polymer. *J Adv Ceram* 2022, **11**: 523–531.

[8] Liu BS, Gu YP, Ji YC, *et al.* Fabrication and mechanical properties of boron nitride nanotube reinforced boron carbide ceramics. *J Ceram Soc Jpn* 2021, **129**: 187–194.

[9] Chen YF, Bi JQ, Yin CL, *et al.* Microstructure and fracture toughness of graphene nanosheets/alumina composites. *Ceram Int* 2014, **40**: 13883–13889.

[10] Wang WL, Bi JQ, Sun KN, *et al.* Fabrication of alumina ceramic reinforced with boron nitride nanotubes with improved mechanical properties. *J Am Ceram Soc* 2011, **94**: 3636–3640.

[11] Wang WL, Bi JQ, Wang SR, *et al.* Microstructure and mechanical properties of alumina ceramics reinforced by boron nitride nanotubes. *J Eur Ceram Soc* 2011, **31**: 2277–2284.

[12] Hu F, Xie ZP, Zhang J, *et al.* Promising high-thermal-conductivity substrate material for high-power electronic device: Silicon nitride ceramics. *Rare Met* 2020, **39**: 463–478.

[13] Wang EY, Shi ZT, Chen MM, *et al.* Investigation of effective thermal conductivity of SiC foam ceramics with various pore densities. *Open Phys* 2022, **20**: 58–65.

[14] Watari K. Evaluation of thermal conductivity of grains and fillers by using thermoreflectance technique—Si_3N_4, AlN, SiC—. *J Ceram Soc Jpn* 2014, **122**: 967–970.

[15] Wang DD, Wang CB, Li MJ, *et al.* Effect of NH_4F additive on purification of AlN ceramics. *J Mater Sci Mater Electron* 2017, **28**: 6731–6736.

[16] Liu ZT, Zhao SQ, Yang T, *et al.* Improvement in mechanical properties in AlN-h-BN composites with high thermal conductivity. *J Adv Ceram* 2021, **10**: 1317–1325.

[17] Lun HL, Zeng Y, Xiong X, *et al.* The effect of SiC content on microstructure and microwave heating rate of h-BN/SiC ceramics fabricated by spark plasma sintering. *Materials* 2019, **12**: 1909.

[18] Li HB, Zheng YT, Han JC, *et al.* Microstructure, mechanical properties and thermal shock behavior of h-BN–AlN ceramic composites prepared by combustion synthesis. *J Alloys Compd* 2011, **509**: 1661–1664.

[19] Chen H, Xu CH, Xiao GC, *et al.* Synthesis of (h-BN)/SiO_2 core–shell powder for improved self-lubricating ceramic composites. *Ceram Int* 2015, **42**: 5504–5511.

[20] Ding D, Yan B, Wang Y, *et al.* Fabrication of h-BN/SiO_2 nanofibers showing high olefins productivity in oxidative dehydrogenation of propane. *ChemCatChem* 2021, **13**: 3312–3318.

[21] Yang XN, Bi JQ, Liang GD, *et al.* The effect of boron nitride nanosheets on the mechanical and thermal properties of aluminum nitride ceramics. *Int J Appl Ceram Tec* 2022, **19**: 2817–2825.

[22] Sun Y, Meng QC, Jia DC, *et al.* Effect of hexagonal BN on the microstructure and mechanical properties of Si_3N_4 ceramics. *J Mater Process Technol* 2007, **182**: 134–138.

[23] Wei DQ, Meng QC, Jia DC. Mechanical and tribological properties of hot-pressed h-BN/Si_3N_4 ceramic composites. *Ceram Int* 2006, **32**: 549–554.
[24] Li MJ, Wang CY, Wang GQ, *et al.* Research progress and trend on preparation techniques of nitride ceramic powders. *Advanced Ceramics* 2023, **44**: 173–182.
[25] Crane TP, Cowan BP. Magnetic relaxation properties of helium-3 adsorbed on hexagonal boron nitride. *Phys Rev B* 2000, **62**: 11359–11362.
[26] Li LH, Cervenka J, Watanabe K, *et al.* Strong oxidation resistance of atomically thin boron nitride nanosheets. *ACS Nano* 2014, **8**: 1457–1462.
[27] Li LH, Chen Y. Atomically thin boron nitride: Unique properties and applications. *Adv Func Mater* 2016, **26**: 2594–2608.
[28] Lorrette C, Weisbecker P, Jacques S, *et al.* Deposition and characterization of hex-BN coating on carbon fibres using tris(dimethylamino) borane precursor. *J Eur Ceram Soc* 2007, **27**: 2737–2743.
[29] Miller M, Owens FJ. Tuning the electronic and magnetic properties of boron nitride nanotubes. *Solid State Commun* 2011, **151**: 1001–1003.
[30] Ji YC, Mao WH, Liao HJ, *et al.* Boron nitride nanotube-nanosheet hierarchical structures and its optical/adsorption properties. *Chem J Chin Univ* 2019, **40**: 216–223. (in Chinese)
[31] Liang P, Li SY. Synthesis, characterization and standard molar enthalpies of formation of two zinc borates: 2ZnO·$2B_2O_3$·$3H_2O$ and ZnB_4O_7. *J Chem Thermodyn* 2019, **139**: 105868.
[32] Li CW, Long XY, E S, *et al.* Magnesium-induced preparation of boron nitride nanotubes and their application in thermal interface materials. *Nanoscale* 2019, **11**: 11457–11463.
[33] Chen Y, Miao CY, Xie SX, *et al.* Fracture behaviors and ferroelastic deformation in W/Cr Co-doped $Bi_4Ti_3O_{12}$ ceramics. *J Am Ceram Soc* 2016, **99**: 2103–2109.
[34] Chen Y, Li LF, Zhou Z, *et al.* La_2O_3-modified $BiYbO_3$–Pb(Zr,Ti)O_3 ternary piezoelectric ceramics with enhanced electrical properties and thermal depolarization temperature. *J Adv Ceram* 2023, **12**: 1593–1611.
[35] Wang JL, Zhang LP, Zhao GW, *et al.* Selective synthesis of boron nitride nanotubes by self-propagation high-temperature synthesis and annealing process. *J Solid State Chem* 2011, **184**: 2478–2484.
[36] Pandey KK, Singh S, Choudhary S, *et al.* Microstructural and mechanical properties of plasma sprayed boron nitride nanotubes reinforced alumina coating. *Ceram Int* 2021, **47**: 9194–9202.
[37] Song KX, Wu SY, Chen XM. Effects of Y_2O_3 addition on microwave dielectric characteristics of Al_2O_3 ceramics. *Mater Lett* 2007, **61**: 3357–3360.
[38] Wang XY, Lv JQ, Xu Y, *et al.* Dielectric responses and structure–property relationships of $Ca_{1-x}Ba_xWO_4$ composite microwave dielectric ceramics. *J Alloys Compd* 2022, **925**: 166669.
[39] Kim J, Hwang S, Sung W, *et al.* Effect of anorthite and diopside on dielectric properties of Al_2O_3/glass composite based on high strength of LTCC substrate. *J Mater Sci* 2008, **43**: 4009–4015.
[40] Lee SJ, Kriven WM. Fabrication of low thermal expansion and low dielectric ceramic substrates by control of microstructure. *J Ceram Process Res* 2003, **4**: 118–121.
[41] Li B, Xu Y, Zhang SR. The size-effect of Al_2O_3 on the sinterability, microstructure and properties of glass–alumina composites. *Glass Phys Chem* 2015, **41**: 503–508.
[42] Ryu BK, Rew SC, Park HC, *et al.* Sintering temperature and dielectric constant of glass–alumina composite with NaF addition. *J Mater Sci Lett* 1996, **15**: 889–891.
[43] Suzdal'tsev EI, Rozhkova TI. Materials with controlled dielectric constants based on a glass ceramic of lithium alumina–silicate composition. *Refract Ind Ceram* 2003, **44**: 260–262.
[44] Fang X, Jiang L, Pan LM, *et al.* High-thermally conductive AlN-based microwave attenuating composite ceramics with spherical graphite as attenuating agent. *J Adv Ceram* 2021, **10**: 301–319.
[45] Chen WZ, Yu YL, Gu YP, *et al.* Controllable synthesis of boron nitride submicron tubes and their excellent mechanical property and thermal conductivity applied in the epoxy resin polymer composites. *Compos Part A Appl Sci Manuf* 2022, **154**: 106783.
[46] Mustafa T, Liu YP, Gao J, *et al.* Highly aligned reduced graphene oxide in alumina composites for strengthening, toughening, and electromagnetic interference shielding. *J Materiomics* 2023, **9**: 993–1003.
[47] Luo W, Wang MY, Wang KJ, *et al.* A robust hierarchical MXene/Ni/aluminosilicate glass composite for high-performance microwave absorption. *Adv Sci* 2022, **9**: 2104163.
[48] Fan YC, Song EH, Mustafa T, *et al.* Liquid-phase assisted engineering of highly strong SiC composite reinforced by multiwalled carbon nanotubes. *Adv Sci* 2020, **7**: 2002225.
[49] Klimczyk P, Wyżga P, Cyboroń J, *et al.* Phase stability and mechanical properties of Al_2O_3–cBN composites prepared via spark plasma sintering. *Diam Relat Mater* 2020, **104**: 107762.
[50] Jaafar M, Bonnefont G, Fantozzi G, *et al.* Intergranular alumina–SiC micro-nanocomposites sintered by spark plasma sintering. *Mater Chem Phys* 2010, **124**: 377–379.
[51] Zhu J, Jia B, Di YJ, *et al.* Effects of graphene content on the microstructure and mechanical properties of alumina-based composites. *Front Mater* 2022, **9**: 965674.
[52] Yin ZZ, Liang GD, Bi JQ. High strength and hardness BNNSs/Al_2O_3 composite ceramics prepared by hot-press sintering of *in situ* composite BNNSs/Al_2O_3 powder. *Ceram Int* 2023, **49**: 31794–31801.